

Original Article

Predicting stomatal responses to the environment from the optimization of photosynthetic gain and hydraulic cost

John S. Sperry¹, Martin D. Venturas¹, William R. L. Anderegg¹, Maurizio Mencuccini^{2,3}, D. Scott Mackay⁴, Yujie Wang¹ & David M. Love¹¹Department of Biology, University of Utah, 257 S 1400E, Salt Lake City, UT 84112, USA, ²School of GeoSciences, University of Edinburgh, West Mains Road, Edinburgh EH9 3Jn, UK, ³ICREA at CREAM, Cerdanyola del Vallès, Barcelona 08193, Spain and ⁴Department of Geography, State University of New York, Buffalo, NY 14260, USA

ABSTRACT

Stomatal regulation presumably evolved to optimize CO₂ for H₂O exchange in response to changing conditions. If the optimization criterion can be readily measured or calculated, then stomatal responses can be efficiently modelled without recourse to empirical models or underlying mechanism. Previous efforts have been challenged by the lack of a transparent index for the cost of losing water. Yet it is accepted that stomata control water loss to avoid excessive loss of hydraulic conductance from cavitation and soil drying. Proximity to hydraulic failure and desiccation can represent the cost of water loss. If at any given instant, the stomatal aperture adjusts to maximize the instantaneous difference between photosynthetic gain and hydraulic cost, then a model can predict the trajectory of stomatal responses to changes in environment across time. Results of this optimization model are consistent with the widely used Ball–Berry–Leuning empirical model ($r^2 > 0.99$) across a wide range of vapour pressure deficits and ambient CO₂ concentrations for wet soil. The advantage of the optimization approach is the absence of empirical coefficients, applicability to dry as well as wet soil and prediction of plant hydraulic status along with gas exchange.

Key-words: Ball–Berry–Leuning model; Cowan–Farquhar optimization; hydraulic limitations; photosynthetic optimization; plant drought responses; plant gas exchange; stomatal modelling; stomatal regulation; xylem cavitation.

INTRODUCTION

Land plants face a fundamental carbon-for-water trade-off. They must open their stomata for photosynthetic gain, but doing so promotes water loss. Plant responses to environment represent a balancing act that presumably optimizes this trade-off in some manner (Cowan & Farquhar 1977; Katul *et al.* 2010; Manzoni *et al.* 2011; Medlyn *et al.* 2011; Bonan *et al.* 2014; Prentice *et al.* 2014). When air and soil are dry, photosynthesis is sacrificed in favour of reduced water loss (Schulze & Hall 1982). When ambient CO₂ is scarce, greater water loss is tolerated in favour of photosynthesis (Morison

1987). The trade-off has seemingly resulted in tight coordination between capacity to supply and transpire water (hydraulic conductance, k , and diffusive conductance to water vapour, G_w) and the maximum capacity for photosynthesis (carboxylation rate, V_{max} , and electron transport rate, J_{max} ; Brodribb *et al.* 2002). If the fulcrum on which this trade-off balances could be identified, it would greatly simplify the difficult problem of predicting how plant gas exchange responds to environmental cues (Prentice *et al.* 2014). In this paper, we describe such a balancing point, explain how it can be readily quantified from measurable plant traits and processes, and evaluate the resulting patterns in stomatal regulation of gas exchange and xylem pressure.

The utility of a stomatal optimization framework has long been recognized, but uncertainty in the optimization criteria and its relation to true fitness costs and benefits has limited its potential for understanding and modelling stomatal behaviour, particularly in response to drying soil. A long-standing theory (Cowan & Farquhar 1977) assumes stomatal regulation maximizes cumulative photosynthesis (A) for a fixed amount of water transpired (cumulative E) over a time period. This is a ‘constrained-optimization’ problem (total E is constrained) whose solution specifies a constant Lagrangian multiplier, λ' , which equals a constant $\partial E/\partial A$. Stomata are assumed to maintain $\partial E/\partial A = \lambda'$ at every instant throughout the time period, and this behaviour can be modelled (Cowan & Farquhar 1977; Cowan 1982; Makala *et al.* 1996; Medlyn *et al.* 2011; Manzoni *et al.* 2013). But a persistent problem is in putting an *a priori* number on λ' . Which of the infinite values for $\partial E/\partial A$ is the right one? The $\partial E/\partial A$ is assumed to represent the ‘unit marginal cost’ ($\partial \text{cost}/\partial \text{gain}$) where the cost of stomatal opening is equated with E and A is the gain (Cowan 1982; p. 591). But it has been challenging to specify the optimal marginal cost, and how it might vary with species, environment and time (Givnish 1986; Manzoni *et al.* 2011; Manzoni *et al.* 2013; Buckley *et al.* 2016).

A related issue is whether the optimization problem is properly framed (Wolf *et al.* 2016). Instead of maximizing photosynthesis for an arbitrarily fixed amount of water loss over some period of time, is it not more to the point that plants would maintain the greatest carbon gain relative to the actual cost of water loss at all times, regardless of the amount of water used or time period involved? Such plants will use more water when

Correspondence: J. S. Sperry. e-mail: j.sperry@utah.edu

it is cheap and there is opportunity for more photosynthetic gain, and they will use less water when its cost rises or there is less photosynthetic opportunity. In this ‘profit maximization’ optimization, there is no arbitrary constraint on the amount of water the plant can use over time, and there is no constant Lagrangian multiplier involved in its solution (no λ'). The equation is: profit = gain – cost. Maximum profit is found by setting the derivative of this equation to zero, at which point $\partial \text{cost} / \partial \text{gain} = 1$. In profit maximization, the unit marginal cost should always equal 1. But to implement this scheme, the cost of water use must be specified.

After the leaf scale concept of coupled carbon and water economy arose we have learned how xylem cavitation limits the transpiration stream (Tyree & Sperry 1988; Sperry *et al.* 1998; Sperry & Love 2015). As the physiological importance of cavitation became accepted, a second perspective on stomatal regulation emerged, which is that stomata act to maximize photosynthesis under the constraint of avoiding excessive xylem cavitation (Feild & Holbrook 1989; Sparks & Black 1999; Tombesi *et al.* 2015; Novick *et al.* 2016). It is possible to model stomatal behaviour in response to water stress solely on the principle that stomata close in proportion to the threat of cavitation on canopy water supply (Sperry & Love 2015; Sperry *et al.* 2016). While this hydraulic approach may prove practical in many applications, it ignores the role of stomata in regulating and responding to photosynthesis, and it does not emerge explicitly from the carbon-for-water tradeoff. However, it does identify the loss of conductivity to cavitation as an important fitness cost of moving water. Mortality is the ultimate fitness cost, and it exhibits a strong linkage to vascular dysfunction (Kukowski *et al.* 2013; McDowell *et al.* 2013; Anderegg *et al.* 2015; Anderegg *et al.* 2016).

Perhaps, the hydraulic models are providing a proxy for the cost of water loss, thus allowing the implementation of the profit maximization theory. Hydraulics provide a ‘cost’ function for stomatal opening, and the corresponding photosynthetic ‘gain’ function can be obtained from trait- and process-based models of photosynthesis. The stomatal regulation that maximizes the profit (where $\partial \text{cost} / \partial \text{gain} = 1$) can be modelled on this basis. In this paper, we develop this perspective and explore its potential for improving our understanding and ability to model stomatal responses to environmental forcing. Its predictions are compared to those of a purely hydraulic model for stomatal conductance (Sperry & Love 2015; Sperry *et al.* 2016) and to a widely used empirical model (Ball, Berry, Leuning [BBL]; Leuning 1995). The contrast in stomatal behaviour between profit maximization versus the $\partial E / \partial A = \lambda'$ constrained optimization is discussed.

Stomatal response modelling does need improvement. We can model leaf energy balance, photosynthesis, hydraulic conductance and transpiration reasonably well under any environmental situation *if* the diffusive conductance of the leaf (G_w) is known (Collatz *et al.* 1991; Collatz *et al.* 1992). In lieu of a trait and process-based predictive model for stomatal control of G_w , models have relied on empirical relationships. Conventional formulations employed by land-surface models assume an empirical model for the G_w response to atmospheric vapour pressure deficit (D), photosynthetic rate (A) and ambient

CO_2 concentration (C_a) under wet soil conditions (e.g. the BBL model; Leuning 1995). The wet soil model is scaled with a second empirical model to yield the G_w response to soil water potential (P_s ; Powell *et al.* 2013). Besides the unsatisfying need to rely on empirical coefficients of unknown physiological meaning, these coefficients must be either robust to widely different plant and soil types or else known for relevant functional types. The stomatal response to drying soil is especially challenging (Williams *et al.* 1996; Darmour *et al.* 2010; Manzoni *et al.* 2011; Manzoni *et al.* 2013; Powell *et al.* 2013). Hence, the search continues for a better way to model stomatal responses that is grounded in relevant process and measurable traits.

THE MODEL

The hydraulic cost function

The hydraulic cost function is based on a ‘supply function’ which describes the theoretical steady-state relation between E and canopy xylem pressure (P_c) at a given root zone soil water potential, P_s (Fig. 1a blue E curve for $P_s = 0$; Fig. 1c blue curve for $P_s = -1$ MPa). Supply functions are calculated from soil and xylem vulnerability curves that describe how hydraulic conductance (k) of a soil or plant component declines from its maximum (k_{max}) in response to negative water pressure (P):

$$k = k_{\text{max}} f(P). \quad (1a)$$

For the plant, a two-parameter Weibull function for $f(P)$ describes a wide range of vulnerability curves (Neufeld *et al.* 1992):

$$f(P) = e^{-((-P/b)^c)}, \quad (1b)$$

analogous to the van Genuchten function used for in soil (van Genuchten 1980). The Weibull ‘ b ’ parameter is P at $k/k_{\text{max}} = 0.37$, and c controls whether the curve is a threshold sigmoidal form ($c > 1$) or non-threshold ‘exponential’ curve (c near 1). Transpiration (E) induces a pressure drop (upstream P – downstream $P = P_{\text{up}} - P_{\text{down}}$) across each soil and xylem element. At steady-state, E is the integral of each element’s vulnerability curve from P_{up} to P_{down} (Sperry & Love 2015):

$$E = \int_{P_{\text{up}}}^{P_{\text{down}}} k_{\text{max}} f(P) dP. \quad (2)$$

By integrating across all vulnerability curves in the soil–plant system, the relation between E and a given total $P_s - P_c$ pressure drop can be found. This ‘supply function’ starts at $E = 0$ at $P_c = P_s$, and rises to $E = E_{\text{crit}}$ at $P_c = P_{\text{crit}}$ (Fig. 1a, blue E curve, expressed per leaf area). It is a curve of increasing damage and risk. The curve is steepest and nearly linear at first when pressures are modest and cavitation is minimal. It begins to flatten as cavitation reduces hydraulic conductance and more pressure drop is required to move water. The instantaneous slope of the supply function at P_c is proportional to the hydraulic conductance in the canopy ($k_c \propto \partial E / \partial P_c$; Sperry *et al.* 2016). The k_c declines from a maximum at $E = 0$ (k_{cmax}) to near 0 (k_{crit}) at $E = E_{\text{crit}}$ (Fig. 1a, end of blue E curve). The $f(P)$ functions (Eqn 1b and soil van Genuchten curves) do

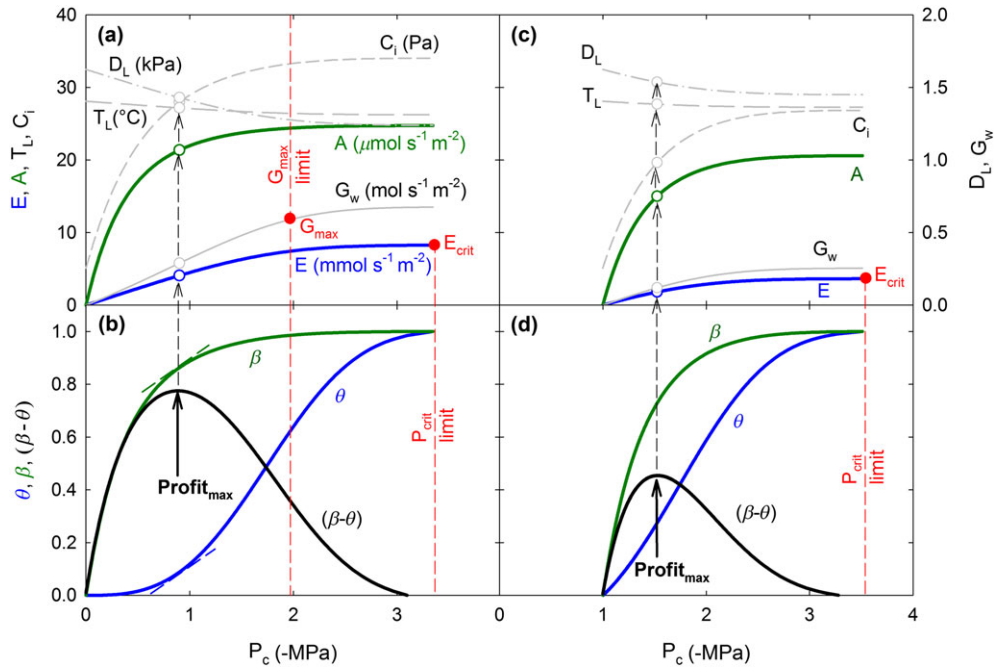


Figure 1. Stomatal response model based on the optimization of photosynthetic gains and hydraulic costs. (a) The blue supply function is the steady state relationship between transpiration (E) and canopy xylem pressure (P_c) that is calculated from the continuum vulnerability curves and soil water potential (P_s). The supply function terminates at E_{crit} (and the associated P_{crit}) beyond which hydraulic failure and canopy desiccation occurs. Under certain conditions (high P_s and low D) maximal diffusive conductance (G_{max}) can limit E and P_c . The E curve is used to calculate consecutively: 1) the leaf temperature (T_L), 2) leaf-to-air vapour pressure deficit (D_L) and 3) diffusive conductance of leaf to water vapour (G_w) and CO_2 (G_c , not shown). The G_c is then used to calculate 4) internal leaf CO_2 concentration (C_i) and 5) the gross assimilation rate (A) from a modelled $A-C_i$ curve. These six curves represent the continuum of possible steady states at a given instant in time. The plant can ‘choose’ any state by adjusting its G_w via stomatal control. (b) The hydraulic cost function (blue θ curve) is the fractional loss of downstream hydraulic conductance that is calculated from the $E(P_c)$ supply function. The θ rises from zero at $P_c = P_s$ to 1 at $P_c = P_{crit}$. The carbon gain function (β) is the fractional increase in A from 0 at $P_c = P_s$ to 1 at its instantaneous maximum as calculated from the $A(P_c)$ curve in (a). Stomata are assumed to maintain the plant at the optimum where $\beta - \theta$ (black curve) is maximized ($Profit_{max}$); $Profit_{max}$ coincides with $\partial\beta/\partial P_c = \partial\theta/\partial P_c$ (tangents on β and θ curves). The optimum specifies P_c and hence the six parameters in (a). (c) The six curves in (a) corresponding to $P_s = -1$ MPa (versus $P_s = 0$ in (a)). (d) The shift in cost (θ) and gain (β) functions associated with $P_s = -1$. The new $\beta - \theta$ optimum predicts the shift in P_c and hence the change in the six parameters in (c).

not go to mathematical zero, so k_{crit} represents a ‘physiological zero’ set to 0.05% of k_{max} : by this point increases in E (beyond E_{crit}) have become undetectable (Fig. 1a). At E_{crit} the supply system has reached its limit: no greater steady-state transpiration rate is possible without driving canopy conductance to zero and desiccating the canopy.

In the hydraulic model of Sperry and Love (Sperry & Love 2015; Sperry *et al.* 2016), stomata are assumed to regulate the $\Delta P = P_s - P_c$ pressure drop based on the fractional drop in canopy hydraulic conductance from its maximum (k_c/k_{cmax}):

$$\Delta P = \Delta P' \frac{k_c}{k_{cmax}}, \quad (3)$$

where $\Delta P'$ is the unregulated pressure drop. This regulated ΔP yields the regulated values for E and P_c , and also the diffusive leaf conductance to water vapour ($G_w = E/D_L$; D_L is leaf-to-air vapour pressure deficit; G_w includes stomatal and boundary layer components). As $\Delta P'$ increases, ΔP rises to a maximum and then falls as k_c/k_{cmax} approaches zero. The hydraulic model assumes ΔP saturates at the maximum, consistent with the tendency for E and P_c to saturate as D_L increases.

Here, we move beyond the purely hydraulic approach and use the supply function to derive a transpirational ‘cost function’ ($\theta(P_c)$) that reflects the increasing damage from cavitation and greater difficulty of moving the transpiration stream:

$$\theta(P_c) = \frac{k_{cmax} - k_c(P_c)}{k_{cmax} - k_{crit}}, \quad (4)$$

where k_c is evaluated at P_c . The θ is the fractional loss of canopy (downstream) hydraulic conductance, which rises to $\theta = 1$ at hydraulic failure. As shown in Fig. 1b (blue θ curve, see also Fig. 1d for $P_s = -1$ MPa), θ rises relatively slowly from zero at $P_c = P_s$ ($k_c = k_{cmax}$) because limited cavitation at modest P_c means water is cheap. However, as P_c becomes more negative and more cavitation is induced, θ accelerates before gradually approaching 1 at $P_c = P_{crit}$ ($k_c = k_{crit}$) where the plant pays the ultimate cost of canopy desiccation. The normalization removes units and relates cost to hydraulically defined end-points corresponding to a particular species (e.g. P_{crit}) and a specific point in time (root zone P_s).

The model of Sperry *et al.* 2016 was used to compute the supply- and cost functions (Fig. 1, blue curves in (a)–(d)). For all simulations in this paper, their model was run in

unsegmented mode (all xylem components assigned the same Weibull $f(P)$ function), with the xylem being limiting (rhizosphere average resistance of 5%). The model runs in reversible and irreversible cavitation modes, but for the present purpose reversibility was moot because all simulations were run from low to high water stress. The Sperry *et al.* model was revised

to express conductances on a leaf area basis to allow energy balance and photosynthesis calculations ('big-leaf' canopy composed of identical leaves). The revised model is a Visual Basic for Applications macro in Microsoft Excel (code available from the senior author). Hydraulic parameters underlying the supply function are listed in Table 1.

Table 1. Main inputs and outputs of the hydraulic cost and photosynthetic gain optimization model

Abbreviation	Variable or parameter description	Default (test values) ^a	Units
Inputs			
(a) Environmental drivers			
C_a	Atmospheric CO ₂ concentration	40 (15–65)	Pa
D	Atmospheric water pressure deficit	1 (0.10–4.26)	kPa
O_a	Atmospheric O ₂ concentration	21 000	Pa
P_{atm}	Atmospheric air pressure	101.3	kPa
P_s	Soil water potential	0 (to –7)	MPa
Q	PAR photon flux density	2000 (0–2000)	$\mu\text{mol s}^{-1} \text{m}^{-2}$
T_A	Air temperature	25 (30 ^b , 10–40 ^c)	°C
u	Wind speed	2	m s^{-1}
(b) Hydraulic cost and photosynthetic gain parameters			
c	Curvature of the light response curve	0.9	
c'	Curvature factor for J_c versus J_c limited photosynthesis	0.98	
d	Leaf width \times 0.72	0.0072	m
G_{max}	Maximum diffusive conductance to water vapour	Set by V_{max25}	$\text{mmol s}^{-1} \text{m}^{-2}$
J_{max25}	Maximum electron transport rate at 25 °C	1.67 V_{max25}	$\mu\text{mol s}^{-1} \text{m}^{-2}$
K_c	Michaelis–Menton constant for carboxylation	41 at 25 °C	Pa
K_o	Michaelis–Menton constant for oxygenation	28 202 at 25 °C	Pa
k_{max}	Maximum soil-canopy hydraulic conductance per leaf area	Set by V_{max25}	$\text{mmol s}^{-1} \text{m}^{-2} \text{MPa}^{-1}$
R_{abs}	Absorbed long- and short-wave radiation	740	W m^{-2}
VC	Two parameter $[b, c]$ Weibull vulnerability curve	[2,3] ([1,3], [3,3], [2,1] ^d)	
V_{max25}	Maximum carboxylation rate at 25 °C	100 (25–150)	$\mu\text{mol s}^{-1} \text{m}^{-2}$
A	Quantum yield of electron transport	0.3	mol mol^{-1}
Γ^*	CO ₂ compensation point	4.36 at 25 °C	Pa
e	Emissivity	0.97	
Outputs			
A	Gross assimilation rate		$\mu\text{mol s}^{-1} \text{m}^{-2}$
A_{max}	Instantaneous maximum gross assimilation rate		$\mu\text{mol s}^{-1} \text{m}^{-2}$
C_i	Internal leaf CO ₂ concentration		Pa
D_L	Leaf to air water pressure deficit		kPa
E	Canopy transpiration rate		$\text{mmol s}^{-1} \text{m}^{-2}$
E_{crit}	Transpiration rate limit (values above desiccate the canopy)		$\text{mmol s}^{-1} \text{m}^{-2}$
G_c	CO ₂ diffusive conductance of leaf		$\mu\text{mol s}^{-1} \text{m}^{-2}$
G_w	H ₂ O vapour diffusive conductance of leaf		$\text{mmol s}^{-1} \text{m}^{-2}$
k	Hydraulic conductance (per leaf-area)		$\text{mmol s}^{-1} \text{m}^{-2} \text{MPa}^{-1}$
k_c	Canopy hydraulic conductance (per leaf area)		$\text{mmol s}^{-1} \text{m}^{-2} \text{MPa}^{-1}$
k_{crit}	Canopy hydraulic conductance when E_{crit} is reached		$\text{mmol s}^{-1} \text{m}^{-2} \text{MPa}^{-1}$
k_{cmax}	Maximum canopy hydraulic conductance		$\text{mmol s}^{-1} \text{m}^{-2} \text{MPa}^{-1}$
Profit _{max}	Maximum profit $[(\beta-\theta)_{max}]$, indicating optimal stomatal conductance for current environmental conditions		
P_c	Canopy xylem pressure		MPa
P_{crit}	Canopy xylem pressure at E_{crit}		MPa
ΔP	Regulated pressure drop between soil and canopy		MPa
$\Delta P'$	Unregulated pressure drop between soil and canopy		MPa
T_L	Leaf temperature		°C
β	Carbon gain function used to optimize stomatal response		
θ	Cost function used to optimize stomatal response		

^aDefault values used for testing the model and the range of values used for testing the effect of these variables on the models output.

^bFor the D response test.

^cFor the T_a response test.

^dThis is an exponential curve whereas the others are sigmoidal curves.

The photosynthetic gain function

The water supply function was translated into its corresponding carbon gain function. Figure 1a,b illustrates the step-wise process for the indicated supply function for $P_{\text{soil}}=0$, $D=1$ kPa and $T_a=25^\circ\text{C}$. In a nutshell, E from the supply function is used to compute leaf temperature (T_L) and D_L from energy balance (Fig. 1a, grey dashed T_L and dash-dotted D_L curves). The diffusive conductances of the leaf to water vapour and CO_2 (G_w , G_c , respectively) are obtained from E and D_L (Fig. 1a, solid grey G_w curve). The gross assimilation rate, A , is then obtained from G_c and a modelled $A-C_i$ curve (Fig. 1a, green A curve). A normalized gain function ($\beta(P_c)$) is computed to complement the hydraulic cost function ($\theta(P_c)$, Fig. 1b, green β curve). The gain function is based on gross assimilation, without subtracting respiration, because in parallel with the cost function, its purpose is to represent the instantaneous gain of opening the stomata. The gross gain provides all energy needs, of which leaf respiration is just one. The leaf temperature, T_L ($^\circ\text{C}$), was calculated for each supply-function E (E converted to two-sided leaf area basis; Campbell & Norman 1998, Eqns 14.1, 14.3) using the linearized expression:

$$T_L = T_A + \frac{R_{\text{abs}} - \varepsilon\sigma T_a^4 - \lambda E}{C_p(g_r + g_{\text{Ha}})}, \quad (5)$$

where R_{abs} is absorbed long- and short-wave radiation (W m^{-2}), ε is emissivity (0.97), σ is the Stefan-Boltzman constant ($5.67 \text{ E} - 8 \text{ W m}^{-2} \text{ }^\circ\text{K}^{-4}$), T_a is mean air temperature in $^\circ\text{K}$ (T_A is in $^\circ\text{C}$), λ is latent heat of vaporization (J mol^{-1}), C_p is specific heat capacity of dry air at constant pressure ($29.3 \text{ J mol}^{-1} \text{ }^\circ\text{C}^{-1}$), g_r and g_{Ha} are radiative and heat conductances ($\text{mol m}^{-2} \text{ s}^{-1}$), respectively, for the leaf. The $g_{\text{Ha}} = 0.189 (u/d)^{-0.5}$, where u is mean windspeed (m s^{-1}) above the leaf boundary layer, and d is set to 0.72-leaf width in m. Temperature dependence of λ and g_r were obtained from Campbell & Norman (1998). Simulations used values in Table 1 unless noted. For constant T_A , leaf temperature falls from a maximum at $E=0$ as transpiration increases (Fig. 1a, grey dashed T_L line).

Leaf temperature was used to calculate G_w , by firstly calculating D_L . The D_L falls from a maximum at $E=0$ as transpiration lowers T_L (Fig. 1a, grey dash-dotted D_L line). The $G_w = E/D_L$ (Fig. 1a, grey solid G_w curve), and $G_c = G_w/1.6$. The portion of the curves to the right of the vertical G_{max} dashed line in Fig. 1a,b corresponds to E above a limit set by a maximum G_w of the leaf (e.g. G_{max} for maximal stomatal opening at the prevailing boundary layer conductance). The G_{max} quickly becomes non-limiting as soil dries (e.g. Fig. 1c,d for $P_s = -1$ MPa) or D increases. Cuticular water loss was assumed zero for present purposes of modelling G_w , because it only influences results at or beyond the point of complete stomatal closure.

With T_L and G_c known, gross A was calculated from established photosynthesis models. Rubisco-limited photosynthesis rate, J_c , was obtained from (e.g. Collatz *et al.* 1991; Medlyn *et al.* 2002):

$$J_c = \frac{V_{\text{max}} (C_i - \Gamma^*)}{C_i + K_c \left(1 + \frac{O_a}{K_o}\right)}, \quad (6)$$

where V_{max} is Rubisco's maximum carboxylation rate ($\mu\text{mol s}^{-1} \text{ m}^{-2}$), C_i is internal CO_2 concentration (Pa), Γ^* is the CO_2 compensation point (Pa), K_c and K_o are Michaelis-Menten constants for carboxylation and oxygenation, respectively, and O_a is atmospheric O_2 concentration (21 000 Pa; K_c , K_o , Γ^* values from Bernacchi *et al.* 2001).

Electron transport-limited photosynthesis, J_e ($\mu\text{mol s}^{-1} \text{ m}^{-2}$), was obtained from Medlyn *et al.* (2002):

$$J_e = \frac{J}{4} \times \frac{C_i - \Gamma^*}{C_i + 2\Gamma^*} \quad (7a)$$

$$J = \frac{\alpha Q + J_{\text{max}} - \left((\alpha Q + J_{\text{max}})^2 - 4c\alpha Q J_{\text{max}}\right)^{0.5}}{2c}, \quad (7b)$$

where α is the quantum yield of electron transport (assumed at $0.3 \text{ mol photon mol}^{-1} \text{ e}$), $Q = \text{PAR}$ photon flux density ($\mu\text{mol s}^{-1} \text{ m}^{-2}$), J is the actual rate of electron transport ($\mu\text{mol s}^{-1} \text{ m}^{-2}$), J_{max} is the maximum rate of electron transport ($\mu\text{mol s}^{-1} \text{ m}^{-2}$) and c defines the curvature of the light response curve (0.9).

The gross assimilation rate at a given C_i is the minimum value of J_e and J_c . To obtain a smooth A versus C_i curve we used (Collatz *et al.* 1991):

$$A = \frac{J_e + J_c - \left((J_e + J_c)^2 - 4c'J_eJ_c\right)^{0.5}}{2c'}, \quad (8)$$

where c' is a curvature factor (0.98).

The temperature dependence of K_o , K_c and Γ^* relative to 25°C was modelled as in Bernacchi *et al.* (2001) and Medlyn *et al.* (2002). The temperature dependence of J_{max} and V_{max} relative to 25°C ($J_{\text{max}25}$ and $V_{\text{max}25}$, respectively) was modelled using Leuning (2002) (his equation 1 with parameters from his Table 2). We assumed $V_{\text{max}25}$ and $J_{\text{max}25}$ co-varied, using $J_{\text{max}25} = V_{\text{max}25} \cdot 1.67$ (Medlyn *et al.* 2002).

The only unknown variable in Eqn 8 is C_i . However, we know G_c from the supply function, which gives a second equation for A :

$$A = \frac{G_c (C_a - C_i)}{P_{\text{atm}}}, \quad (9)$$

where C_a is atmospheric CO_2 concentration (40 Pa) and P_{atm} is atmospheric pressure (101.3 kPa). We set Eqns 9 and 8 equal to each other and solved for C_i , thereby obtaining A . Both C_i and A rise steeply with G_w before approaching saturation (Fig. 1a, grey dashed C_i curve and green A curve for parameter values listed in Table 1).

A normalized photosynthetic gain function ($\beta(P_c)$) was calculated as

$$\beta(P_c) = \frac{A(P_c)}{A_{\text{max}}}, \quad (10)$$

where A is evaluated at P_c , and A_{max} is the *instantaneous* maximum A over the full P_c range from $P_c = P_s$ to $P_c = P_{\text{crit}}$ (not the

Table 2. Ball–Berry–Leuning Model fits (BBL; Eqn 12; Leuning 1995) to leaf diffusive conductance (G_w) predicted from profit maximization (as plotted in Fig. 8). Means and standard error (in parentheses) given for $n > 1$ simulations

Response	n	r^2	a'	D_o (kPa)	G_o (mol s ⁻¹ m ⁻²)
D_L^a (Fig. 4)	6	0.99738(0.000065)	14.0(0.91)	0.64(0.067)	0.036(0.0063)
D_L (Fig. 7)	11	0.99968(0.000038)	27.5(0.37)	0.213(0.0054)	0.0673(0.00127)
C_a^b (Fig. 7)	5	0.988(0.0038)	36.00790(0.00093)	0.126(0.0037)	0.110(0.0038)
Q^c (Fig. 5)	1	0.91	79.71	0.04	0.16
T_L^d (Fig. 5)	1	0.12	8.59	0.16	0.22
P_s^e (Fig. 6)	6	0.9416(0.00260)	260(165)	0.09(0.034)	-0.0132(0.00212)

^aLeaf-air vapour pressure deficit.

^bAmbient CO₂ concentration.

^cPhotosynthetically active radiation.

^dLeaf temperature.

^eSoil water potential.

biochemical A_{\max}). The gain function rises steeply from $\beta = 0$ at $P_c = P_s$ as stomata open before flattening to $\beta = 1$ as P_c becomes more negative and photosynthesis saturates (Fig. 1b, green β curve). Like the $\theta(P_c)$ cost function, the gain function is normalized by the extremes, making it dimensionless, and relevant only to the moment in time for which it is computed.

It is important to know that the family of $f(P_c)$ curves in Fig. 1a,b [$E(P_c)$, $T_L(P_c)$, $D_L(P_c)$, $G_w(P_c)$, $C_i(P_c)$, $A(P_c)$, $\theta(P_c)$, $\beta(P_c)$] represent steady-state values at a fixed instant where root zone P_s , atmospheric D , air temperature (T_a), wind speed (u) and light level (Q) are frozen in time. The plant can only occupy one stable point on this theoretical constellation of possibilities. At the next time step, gradual shifts in soil and air moisture, temperature, windspeed and light create a new set of possibilities, only one of which the leaf will ‘target’ via its stomatal response (assuming stomata keep pace with typically gradual changes). Figure 1c,d shows, for example, how these functions shift when P_s drops to -1 MPa. If a simple rule that approximated the presumably adaptive stomatal response can be found, then it becomes possible to anticipate where the plant regulates itself on these gradually shifting curves, assuming approximately steady-state conditions.

Instantaneous profit maximization

Wolf *et al.* (2016) pose the optimization criterion that at each instant in time, the stomata regulate canopy gas exchange and pressure to achieve the maximum profit, which is the maximum difference between the normalized photosynthetic gain and hydraulic cost functions:

$$\text{Profit}_{\max} = [\beta(P_c) - \theta(P_c)]_{\max}. \quad (11a)$$

The maximization is achieved when:

$$\frac{\partial \beta}{\partial P_c} = \frac{\partial \theta}{\partial P_c}. \quad (11b)$$

Note that β and θ can be expressed as functions of G_w instead of P_c because of the coupling evident in Fig. 1. Figure 1b shows the β – θ curve and its maximum (black curve), which coincides with equal gain and cost derivatives (Fig. 1b, green and blue tangent lines to their respective curves). Instantaneous profit

maximization assumes a ‘use it or lose it’ reality with regards to available soil water. Any more conservative water use strategy would backfire when soil water is not safe from competitors (i.e. instantaneous optimizers), drainage or surface evaporation. Although modelling optimization avoids specifying mechanism, β and θ are determined by leaf-level phenomena: A for β , and $\partial E/\partial P_c$ for θ . Plants can sense their photosynthetic status and water balance (Paul & Foyer 2001; Tombesi *et al.* 2015), and hence potentially how both change in response to active control of G_w and E . The steady-state assumption represents the sustainable baseline β and θ . This is most appropriate for middle of day gas exchange, which is generally a good predictor of daily totals (e.g. von Allmen *et al.* 2015).

Because the gain function accelerates more quickly from zero and reaches 1 sooner than the cost function (Fig. 1b, green versus blue curves), their maximum difference occurs at a unique intermediate P_c (Fig. 1b, black β – θ curve), which yields the corresponding solutions for actual E , G_w , A , G_c , C_i , T_L , and D_L at that instant (Fig. 1, dashed arrows from maximum to open symbols on curves in (a)).

As environmental conditions shift, so does the optimum. The influence of drier soil ($P_s = -1$ MPa) is shown in Fig. 1c,d. The cost and gain functions are reset to start from 0 at $P_c = P_s$ and rise to 1, but they rise from a more negative P_s . The rise of the gain function is not materially altered (only via changes in T_L) because we assumed no direct effect of P_c on A . However, the cost function rises more steeply because it is computed from the more curved part of the supply function where more cavitation is occurring. The rapidly rising cost results in a smaller optimal soil-canopy ΔP , and a lower optimal G_w . The Fig. 1 example was computed from a sigmoidal vulnerability curve ($b=2$, $c=3$). As explored under ‘model performance’ the shape of the vulnerability curve influences how P_s changes the cost function shape, and hence how the optimal pressure drop and G_w change with drying soil.

The optimal solution also depends on D , T_A , C_a and light. These environmental variables influence the optimum by changing the shape of the gain function, as discussed under ‘model performance’. When conditions flatten the gain function (e.g. high D , low C_a , high T_A ; Fig. 2a, dashed green curve), the optimum shifts to more negative P_c (dashed black curve) driving an increase in the optimal soil-canopy pressure drop

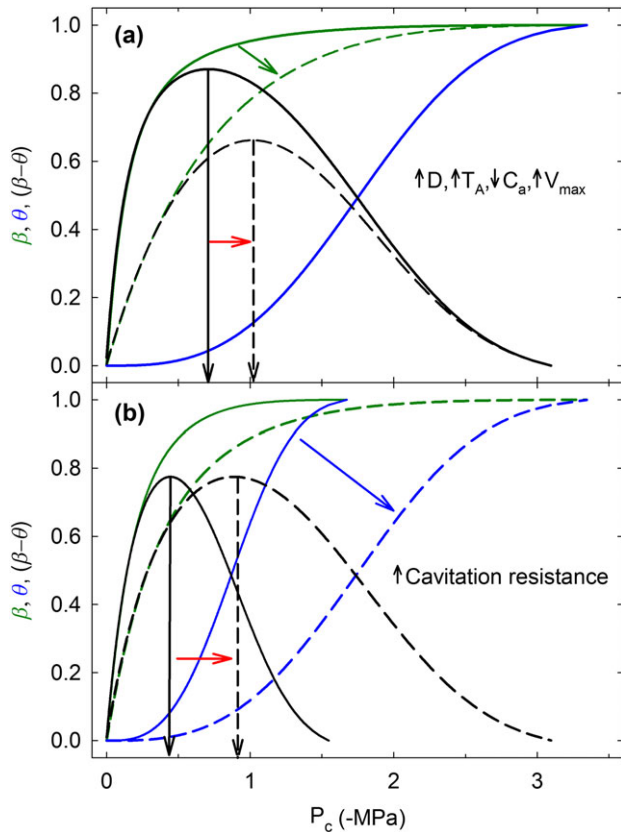


Figure 2. Effects of environment and plant on the cost (θ , blue) and gain (β , green) functions and their difference ($\beta-\theta$, black). (a) The gain function shifts in the direction of the green arrow if there is an increase in vapour pressure deficit (D), air temperature (T_A ; at or below photosynthetic optimum), or maximum carboxylation rate (V_{\max}), or a decrease in ambient CO_2 concentration (C_a). This results in a shift of the optimum (black arrows) in the direction of the red arrow. The cost function is not affected by changes in these variables. (b) The cost function shifts in the direction of the blue arrow as cavitation resistance increases, resulting in a shift of the optimum (black arrows) in the direction indicated by the red arrow. The gain function also shifts with the soil-canopy vulnerability curve change because of differences in leaf temperature.

(Fig. 2a, red arrow, dashed vertical arrow). When conditions steepen the gain function (e.g. low D , high C_a , low T_A ; Fig. 2a solid green curve), the optimum results in less negative P_c (solid black curve) and a smaller soil-canopy pressure drop (Fig. 2a, solid vertical arrow).

The key plant traits that influence the optimum include the vulnerability curve (Weibull b , c parameters), the maximum soil-canopy hydraulic conductance (k_{\max}) and leaf diffusive conductance (G_{\max}), and the photosynthetic capacity ($V_{\max25}$). More vulnerable xylem creates a faster rise in the cost function and forces a less negative optimal P_c (Fig. 2b, solid curves for vulnerable xylem versus dashed for resistant). A higher k_{\max} and G_{\max} increase E and G_w for a given optimal P_c . A greater $V_{\max25}$ creates a slower rise in the gain function and drives optimal P_c to a more negative value (Fig. 2a, dashed curves; see also Fig. S1d). As described next, the model predicts that these plant traits should be highly coordinated.

Longer-term optimization of photosynthetic and hydraulic parameters

Employing the instantaneous optimization scheme to solve for plant gas exchange reveals a second scale of optimal coordination between photosynthetic capacity ($V_{\max25} = J_{\max25}/1.67$), maximum hydraulic capacity (maximum soil-canopy hydraulic conductance, k_{\max} (expressed per leaf area), and maximum diffusive conductance (G_{\max}). Assuming firstly that G_{\max} is not limiting, if k_{\max} is set too low relative to $V_{\max25}$, the instantaneously optimal E and G_c are low, and G_c limits the optimum A (Fig. 3a, solid A curves for $V_{\max25} = 25$ versus $150 \mu\text{mol s}^{-1} \text{m}^{-2}$) even under the most favourable conditions

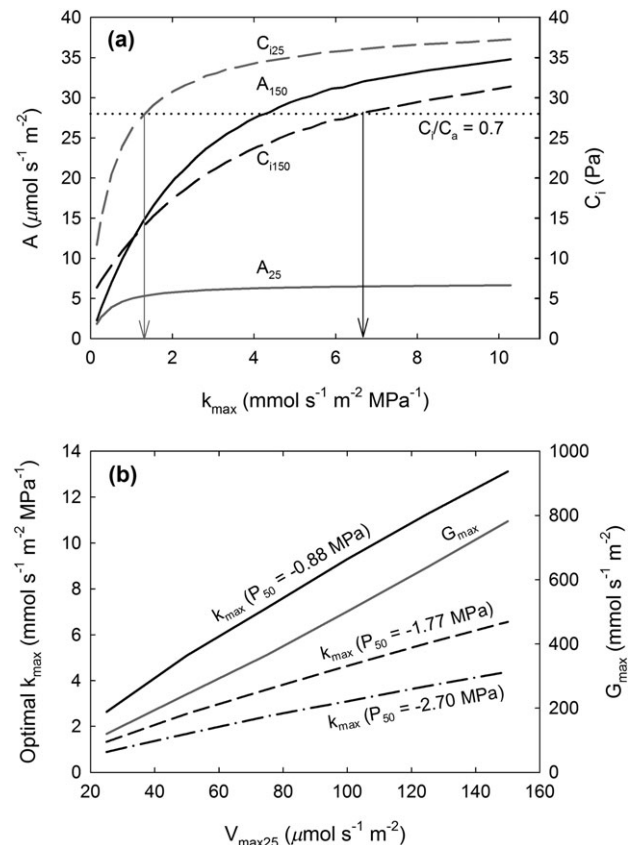


Figure 3. Optimal coordination among soil-canopy maximum hydraulic conductance (k_{\max}), maximum diffusive conductance (G_{\max}) and photosynthetic capacity ($V_{\max25}$). (a) Instantaneous optimal gross assimilation rate (A) for two maximum carboxylation rates ($V_{\max25}$): $25 \mu\text{mol s}^{-1} \text{m}^{-2}$ (A_{25} , solid grey curve) and $150 \mu\text{mol s}^{-1} \text{m}^{-2}$ (A_{150} , solid black line) calculated for different values of k_{\max} . The leaf internal CO_2 concentrations (C_i) corresponding to these instantaneous optimum assimilation rates are also represented for A_{25} (C_{i25} , broken grey curve) and A_{150} (C_{i150} , broken black curve). Optimal k_{\max} for each $V_{\max25}$ (vertical arrows) is determined when the $C_i/C_a = 0.7$ (intersection of C_i curves with black dotted $C_i/C_a = 0.7$ line; $C_a = 40 \text{ kPa}$). (b) The optimal k_{\max} (black curves) increases with $V_{\max25}$, and also increases with more vulnerable xylem (as indicated by higher P_{50} , which is the xylem pressure at which 50% of conductivity loss is reached). The Weibull parameters [b,c] for the three curves represented were [1,3] for $P_{50} = -0.88 \text{ MPa}$, [2,3] for $P_{50} = -1.77 \text{ MPa}$ and [3,3] for $P_{50} = -2.70 \text{ MPa}$. The optimal G_{\max} increases with $V_{\max25}$ (grey line), but does not change with xylem vulnerability.

(Fig. 3a assumes full sunlight, $D = 1$ kPa, $P_{\text{soil}} = 0$ MPa, $T_a = 25^\circ\text{C}$). Greater k_{max} causes G_c to increase, allowing the instantaneous optimum A to rise and saturate for a given $V_{\text{max}25}$ setting (Fig. 3a, solid A curves). The rise along a given optimal A curve is paralleled by a rise in C_i (Fig. 3a, dashed C_i curves accompanying respective A curves). Over the long term, a plant should invest in sufficiently large k_{max} to nearly saturate the instantaneous optimum A under favourable conditions. Too low k_{max} would fail to realize maximum photosynthetic potential; too high k_{max} would be wasted on negligible return. The theory predicts near saturated optimal A at a C_i/C_a ratio of ca. 0.7 (Fig. 3a, dotted $C_i/C_a = 0.7$ line; $C_a = 40$ Pa), which is also what is typically observed in C3 plants under favourable conditions (Wong *et al.* 1979; Hetherington & Woodward 2003; Prentice *et al.* 2014). In this paper, the interest is in modelling plant responses to environmental variables, so we used this k_{max} versus V_{max} coordination (plotted in Fig. 3b, black optimal k_{max} curves) to simplify parameterization (k_{max} is set to achieve $C_i = 28$ Pa at $D = 1$ kPa, $P_s = 0$ MPa, $T_A = 25^\circ\text{C}$). Similarly, we chose a G_{max} that was sufficiently high so as not to limit optimal A under favourable conditions, but not overly high. We used G_w at $D = 0.25$ kPa as our G_{max} setting (Fig. 3b, G_{max}).

The optimal k_{max} also depends on the vulnerability of the xylem to cavitation, with more vulnerable xylem requiring higher k_{max} to achieve $C_i/C_a = 0.7$ (Fig. 3b, k_{max} curves for sigmoidal curves [Weibull $c = 3, b = 1, 2, 3$; pressures at 50% loss of conductivity, P_{50} , shown in Fig. 3b]). The reason for this is that cavitation at modest P_c makes the hydraulic cost (θ) rise faster (Fig. 2b, solid blue curve for vulnerable xylem), restricting the optimal soil-canopy ΔP (vertical solid arrow for solid black curve). Low ΔP means low E and G_c . Increasing k_{max} does not change the optimal ΔP much, but it does increase E and G_c , which allows optimal A to rise and C_i/C_a to reach 0.7. The G_{max} corresponding to $C_i/C_a = 0.7$ does not depend on vulnerability (Fig. 3b, single G_{max} curve).

MODEL PERFORMANCE

Responses to environment

In this section, the responses of the optimization model to various environmental factors are examined. We assumed the coordination of $V_{\text{max}25}$, k_{max} and G_{max} as described in the previous section. For each environmental factor, all other parameters were held constant at default values (Table 1) except as noted. We examine the G_w and P_c sensitivity to $V_{\text{max}25}$ settings first ($V_{\text{max}25} = 25$ versus $150 \mu\text{mol s}^{-1} \text{m}^{-2}$), and then to vulnerability curve settings (at $V_{\text{max}25} = 100 \mu\text{mol s}^{-1} \text{m}^{-2}$). For vulnerability curves, we use sigmoidal curves (Weibull $c = 3$, varying b from 1 to 3) and also explore the change in curve shape from sigmoidal ($c = 3$) to exponential ($c = 1$) while holding $b = 2$. We compare the carbon versus water optimization solution with the purely hydraulic solution from the model of Sperry *et al.* 2016 for the same settings, using Eqn 3 instead of Eqn 11 to locate the plant on the $E(P_c)$, $A(P_c)$, and associated family of $f(P_c)$ functions (Fig. 1a). In a concluding section, we evaluate the fit of the empirical BBL model for each environmental response.

Leaf-to-air vapour pressure deficit, D_L

To obtain the response to D_L , we varied the atmospheric D at a constant $T_A = 30^\circ\text{C}$ (maximum $D = 4.26$ kPa), and $P_s = 0$. Owing to generally higher T_L , this yielded maximum D_L of ca. 4.5 kPa. Higher D_L flattened the $G_w(P_c)$ curve (i.e. the grey G_w curve in Fig. 1a), resulting in a lower optimal G_w and the typical closure response (Fig. 4a). Closure started from an initial G_w that depended on the $V_{\text{max}25}$ setting as described in the previous section. Higher D_L was also associated with a gradual decline in P_c (Fig. 4b). This happened because the flatter $G_w(P_c)$ curve also flattened the gain function, which makes optimal P_c more negative (i.e. as illustrated by the dashed curves in Fig. 2a, see Fig. S1a for a specific example).

The general closure response was similar to that of the hydraulic model, although with two subtle differences. The hydraulic model predicted a smooth transition from G_{max} versus the sharp one for optimization (Fig. 4a, best seen for solid $V_{\text{max}25} = 150$ curve). This difference may be trivial, however, because G_{max} is unlikely to be limiting under typical D_L . The hydraulic model also predicted slightly more closure at high D_L , corresponding to its assumption of achieving perfectly isohydric P_c (Fig. 3b, grey curves). This differs from the aforementioned quasi-isohydric response of the optimization scheme, with P_c creeping to more negative values at high D_L (Fig. 3b, black curves). In general, however, P_c values were in a similar range for the two schemes.

The G_w response to D_L was not sensitive to vulnerability to cavitation for the sigmoidal curves tested (Fig. 4c, solid black curve for $b = 1-3, c = 3$), and this was true for the hydraulic model as well (Fig. 4c, grey curve). The insensitivity results from the insensitivity of G_{max} to sigmoid vulnerability achieved via k_{max} coordination (Fig. 3b). However, for the exponential vulnerability curve, more closure was predicted for all D_L (Fig. 4c, dashed black curve for $b = 2, c = 1$), similar to the hydraulic model prediction (Fig. 4c, dashed grey curve). In both cases, the result is attributable to the steeper initial rise in the cost function associated with cavitation of highly vulnerable xylem at the start of the exponential vulnerability curve (Fig. S2a).

The optimal P_c became significantly more negative in response to greater Weibull b (greater cavitation resistance) at all D_L for the sigmoidal curves (Fig. 4d, solid black curves). This owes to the delayed rise in the cost function with greater sigmoid resistance (as illustrated by dashed curves in Fig. 2b; see also Fig. S1f). The P_c for the exponential curve was relatively modest (Fig. 4d, dashed black curve, $b = 2, c = 1$), again because of the steeper initial rise in the cost function for an exponential versus a sigmoidal curve (Fig. S2a). The hydraulic model predicted similar P_c responses to vulnerability, but with perfect isohydry at high D_L (Fig. 4d, grey solid (b varying) and dashed ($b = 2, c = 1$) curves).

Temperature and light, T_A, T_L, Q

The main effect of temperature on G_w and P_c is via its influence on D_L . However, there was a direct effect of leaf temperature revealed by holding D_L constant. We show just one example,

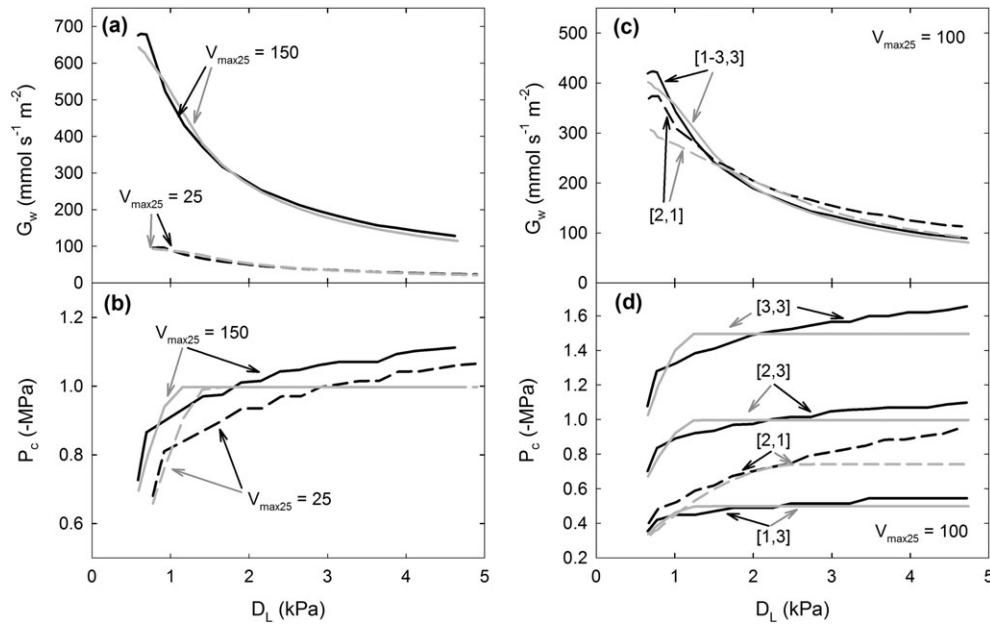


Figure 4. Diffusive vapour conductance (G_w) and xylem canopy pressure (P_c) responses to variations in leaf-to-air vapour pressure deficit (D_L) for the optimization model (black curves) versus the Sperry *et al.* (2016) hydraulic model (grey curves). (a) G_w and (b) P_c response to D_L for both models for two maximum carboxylation rates, $V_{max25} = 25 \mu\text{mol s}^{-1} \text{m}^{-2}$ (dashed curves) and $V_{max25} = 150 \mu\text{mol s}^{-1} \text{m}^{-2}$ (solid curves). (c) G_w and (d) P_c response to D_L for both models for different vulnerability curves (VCs) as determined by the Weibull [b,c] parameters (sigmoidal VCs [1-3,3], solid line; exponential VCs [2,1], dashed lines). All curves were constructed at $T_A = 30^\circ\text{C}$ with other parameters given in Table 1.

keeping D_L constant at ca. 1.5 kPa by varying D , and setting k_{max} to its optimum at $T_A = 25^\circ\text{C}$ and $V_{max} = 100 \mu\text{mol s}^{-1} \text{m}^{-2}$. In the optimization model, G_w , A , E and P_c all respond to temperature, rising to a maximum before falling at high T_L (Fig. 5a, solid black G_w curve, dashed black A curve). The response is caused by the temperature-induced shift in the gain function, from saturation at modest P_c under cool conditions (e.g. represented by the solid green curve in Fig. 2a; see Fig. S1b for specific example) to saturation at more negative P_c under optimal warmth (dashed green curve in Fig. 2a). The hydraulic model shows no temperature response of G_w (nor E or P_c ; Fig. 5a, solid grey G_w line) because its P_c solution is independent of temperature (Eqn 3). The A response, however, is similar to the optimization prediction because the $A(P_c)$ curve is identical between models (Fig. 5a, dashed grey A curve).

The optimization model also responds to light, predicting stomatal closure as Q (PAR) falls to zero (Fig. 5b). The exact G_w by Q trajectory depends on how D , T_A , u and R_{abs} co-vary with Q . For the sake of isolating the light response, we held D , T_A and u constant, but allowed R_{abs} to fall linearly with Q from the default 740W m^{-2} to earth's black body radiation at $Q=0$. The optimization model predicts stomatal closure because lower light causes A to saturate at less negative P_c , which steepens the gain function and results in a less negative optimal P_c . In contrast, the hydraulic model does not predict stomatal closure under low light, because stomata do not respond to A . The A trajectory is similar in both models, falling with Q according to Eqn 7 in both models.

Soil water potential, P_s

With D held constant at 1 kPa ($T_a = 25^\circ\text{C}$), the optimization scheme predicted stomatal closure in response to P_s (Fig. 6a). While some of the closure response is associated with a slight, but inevitable increase in D_L because of less transpirational cooling (from $D_L = 1.3$ to ca. 1.65 kPa), closure was predicted even if D_L was held constant (by manipulating D). The P_s -induced closure resulted from two factors: the generally flatter $E(P_c)$ trajectory caused by dry soil (e.g. compare blue E curves in Fig. 1a versus 1c), and the faster rise in the cost function (e.g. compare blue θ curves in Fig. 1b versus 1d; see also Fig. S1e), which restricts the soil-canopy pressure drop. The closure response starts from higher G_w with greater V_{max25} , consistent with Fig. 4a for the D_L response. If V_{max25} was down-regulated (e.g. Limousin *et al.* 2013) with P_s (to maintain $C_i/C_a = 0.7$), closure was accelerated slightly (Fig. 6, down-regulated curve for initial $V_{max25} = 150 \mu\text{mol s}^{-1} \text{m}^{-2}$). The hydraulic model (Fig. 6a, grey curves) predicted somewhat more gradual closure than the optimization scheme. Both scenarios predicted nearly complete closure at a similar P_s (ca. -3 MPa for the Weibull $b=2$, $c=3$ default vulnerability curve; P_{crit} ca. -4 MPa).

The closure response to P_s was associated with a reduction in P_c that was similar regardless of V_{max25} setting (Fig. 6b, solid black curve). Downregulation of V_{max25} with P_s (Fig. 6b) restricted the drop of P_c , in keeping with the accelerated closure response. A similar restriction on P_c was also seen for the hydraulic model (Fig. 6b, solid grey curve). Both models predicted a gradual reduction in soil-canopy ΔP as soils dried. This ΔP reduction resulted from the steeper cost associated with

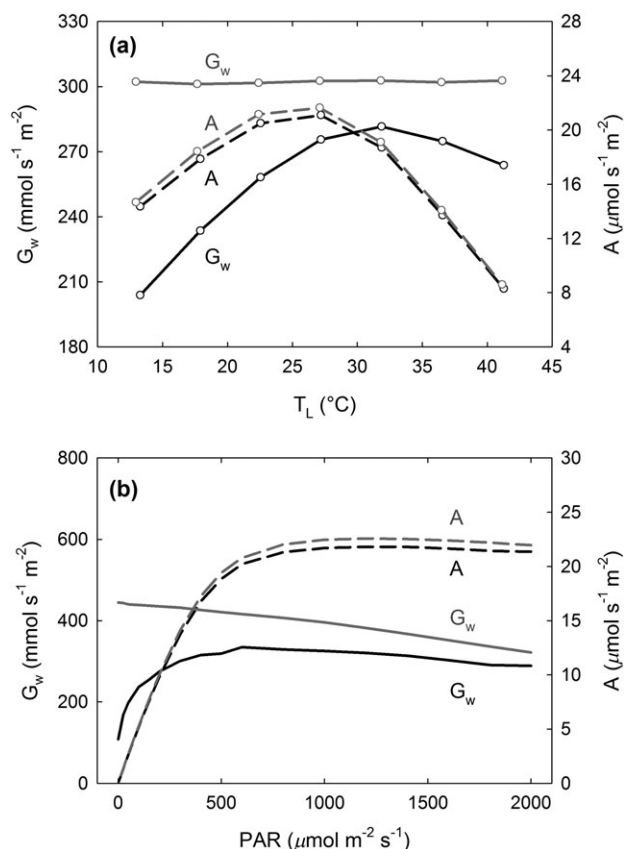


Figure 5. Diffusive vapour conductance (G_w , solid curves) and gross assimilation rate (A , dashed curves) responses to (a) leaf temperature (T_L) and (b) photosynthetic active radiation (PAR) for the optimization model (black curves) and the Sperry *et al.* (2016) hydraulic model (grey curves). The leaf-to-air vapour pressure deficit was held constant, $D_L \approx 1.5$ kPa, by varying D for the T_L response. The absorbed radiation (R_{abs}) was varied proportionally from 447 W m⁻² (the equivalent of Earth's radiation if it were a black body at 25 °C) for PAR = 0 μmol m⁻² s⁻¹ to 740 W m⁻² for PAR = 2000 μmol m⁻² s⁻¹. The remaining parameters are given in Table 1.

more negative P_s for the default sigmoidal vulnerability curve (as illustrated in Fig. 1b,d; see also Fig. S1e).

Vulnerability to cavitation had a major influence on the stomatal sensitivity to P_s . More resistant sigmoidal curves relaxed the cost function (dashed blue line in Fig. 2b; see Fig. S1e for specific example) and resulted in more gradual closure that extended gas exchange to more negative P_s (Fig. 6c, solid black curves). Altering a sigmoidal curve ($b = 2$, $c = 3$) to an exponential one ($b = 2$, $c = 1$) caused even more gradual closure and extension to even more negative P_s (Fig. 6c, dashed black curve). As noted before, exponential curves produce steep cost functions in wet soil because of lots of initial cavitation (Fig. S2a). This causes more stomatal closure (and less negative P_c) than a sigmoidal curve. In dry soil, however, the situation is reversed (Fig. S2b). The long, flat tail of the exponential curve (P_{crit} of ca. -17 MPa) results in a relatively less steep cost function, and hence relatively less closure (and more negative P_c) than a sigmoidal curve. In all cases, the G_w response to vulnerability curves was similar to the hydraulic model (Fig. 3c, solid grey curves for sigmoidal, dashed grey for exponential shape).

The P_c regulation paralleled the G_w trend. More resistant sigmoidal curves resulted in more gradual reduction in the soil-canopy ΔP extending to more negative P_s (Fig. 6d, solid black curves), a trend very similar to the hydraulic model (Fig. 6d, solid grey curves). The exponential curve ($b = 2$, $c = 1$) caused a more restricted ΔP in wet soil, but a gradual increase in ΔP with more negative P_s (Fig. 6d, dashed black curve). Beyond the scale shown in Fig. 6d, the ΔP diminished again, but gas exchange at that point is negligible (Fig. 6c). This exponential ΔP response results from the relatively steep cost function in wet soil that relaxes at intermediate P_s (Fig. S2). The hydraulic model predicts near constant ΔP for the exponential curve (Fig. 6d, dashed grey curve).

CO₂ response, C_a

We computed the CO₂ response by holding V_{max25} constant (100 μmol s⁻¹ m⁻²), setting T_A to 25 °C, and allowing G_{max} to be unlimited (to detect the maximum opening response). The optimization scheme predicted stomatal opening and more negative P_c in response to low atmospheric C_a (<40 Pa), and closure with P_c moderation under high C_a (>40 Pa; Fig. 7). Low CO₂ caused opening because it made the gain function saturate at more negative P_c , thus making optimal P_c more negative, and increasing the optimal E and G_w (i.e. the response represented by the dashed green and black curves in Fig. 2a; see Fig. S1c for an example). High CO₂ caused closure because it caused the gain function to saturate at less negative P_c , making the optimal P_c less negative, along with lower E and G_w (the solid green and black curves in Fig. 2a). Higher V_{max25} and higher temperature (up to the optimum) created a greater CO₂ response than lower V_{max25} and temperature (responses not shown).

The CO₂ response was also greatest at low D (Fig. 1a,b) and less negative P_s (Fig. 1c,d) because these conditions promoted generally high G_w , and hence greater scope for the CO₂ response. High D and negative P_s suppressed G_w and the CO₂ response. Increasing the sigmoidal resistance to cavitation had no effect on the wet soil CO₂ response (i.e. the responses in Fig. 7a,b), but decreased the attenuation in CO₂ response with P_s (i.e. reduced the rate at which the CO₂ response dropped with P_s in Fig. 7c,d).

Comparison to Ball–Berry–Leuning (BBL) model

The BBL model (Leuning 1995) empirically relates G_w (mol s⁻¹ m⁻²) to A (μmol s⁻¹ m⁻²), D_L and C_a :

$$G_w = G_o + \frac{a'A}{(C_s - \Gamma^*) \left(1 + \frac{D_L}{D_o}\right)}, \quad (12)$$

where C_s is the CO₂ concentration at the leaf surface (set to C_a , μmol mol⁻¹, Γ^* in same units), and G_o (mol s⁻¹ m⁻²), a' (dimensionless) and D_o (kPa) are fitted coefficients. The BBL model provided near perfect fits to the optimization G_w for both the D_L and C_a responses from Figs 4 and 7 (Fig. 8a, b; $r^2 \approx 1$). Best-fit coefficients (a' , G_o , D_o ; Table 2) were relatively stable. The light response from Fig. 5b was fit less well

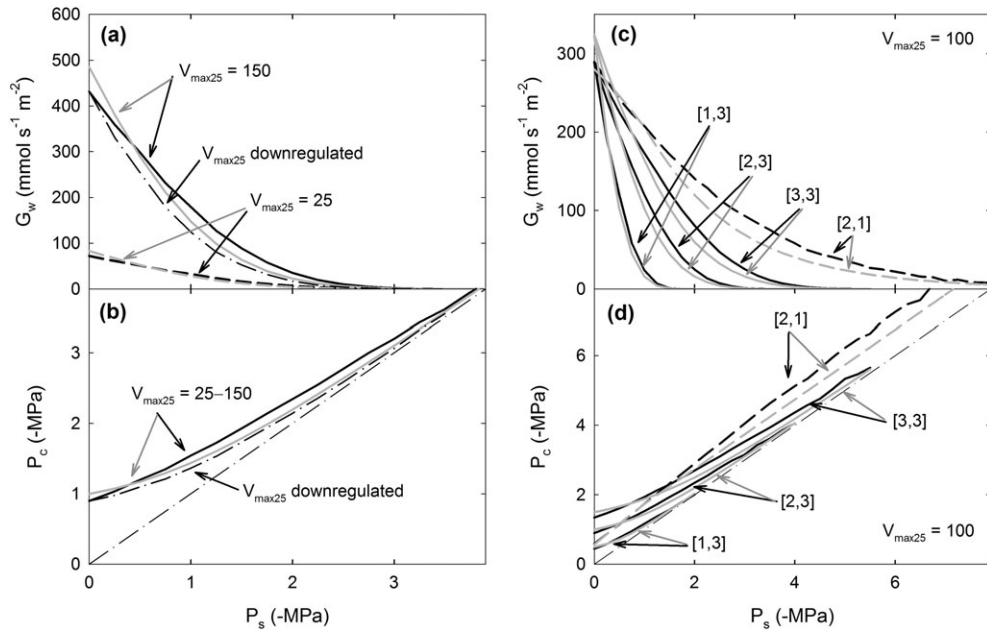


Figure 6. Diffusive vapour conductance (G_w) and xylem canopy pressure (P_c) responses to soil water potential (P_s) of the optimization model (black curves) versus the Sperry *et al.* (2016) hydraulic model (grey curves). (a) G_w response to P_s for both models for two maximum carboxylation rates, $V_{max25} = 25 \mu\text{mol s}^{-1} \text{m}^{-2}$ (dashed curves) and $V_{max25} = 150 \mu\text{mol s}^{-1} \text{m}^{-2}$ (solid curves). Dash-dotted 'downregulated' curve corresponds to reduction in V_{max25} from $150 \mu\text{mol s}^{-1} \text{m}^{-2}$ as required to maintain internal CO_2 at 70% of ambient. (b) P_c response to P_s (the response for both V_{max25} values was equal; dash-dotted represents downregulated V_{max25}). (c) G_w and (d) P_c response to P_s for both models for different vulnerability curves (VCs) as determined by the Weibull [b,c] parameters (sigmoidal VCs [1-3,3], solid curves; exponential VCs [2,1], dashed curves). All other parameters are given in Table 1. The dash-point line represents the 1:1 relation between P_c and P_s .

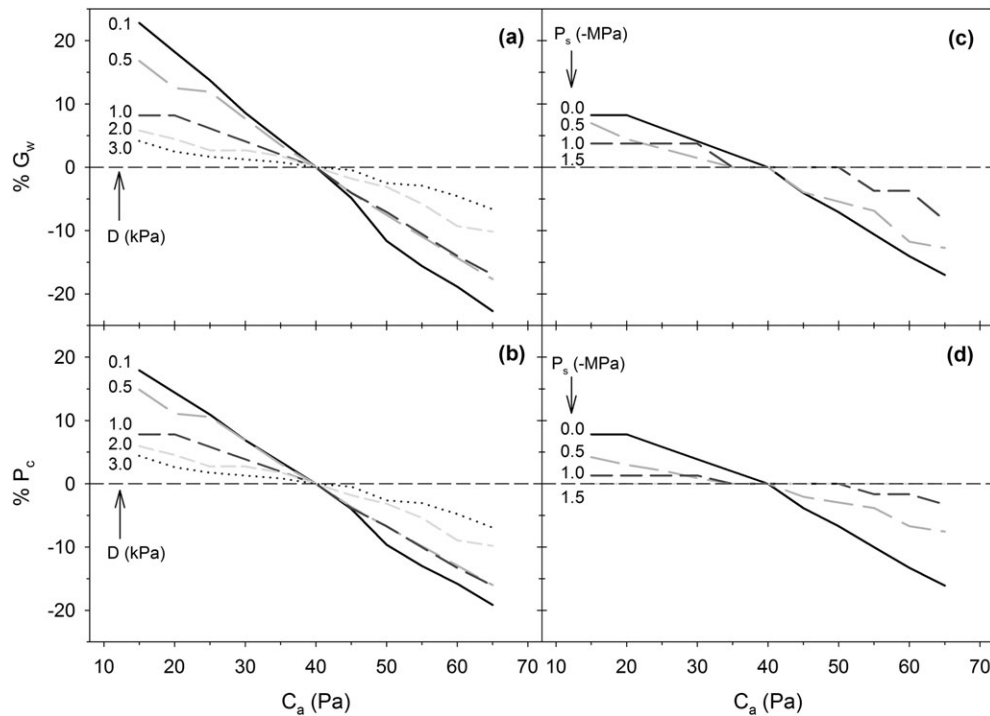


Figure 7. Diffusive conductance (G_w) and canopy xylem pressure (P_c) responses to different atmospheric CO_2 concentrations (C_a). (a) Percent G_w difference relative to G_w at $C_a = 40$ Pa for different air vapour pressure deficits (D). (b) Percent P_c difference relative to P_c at $C_a = 40$ Pa for different air vapour pressure deficits (D). (c) Percent G_w difference relative to G_w at $C_a = 40$ Pa for different soil water potentials (P_s). (d) Percent P_c difference relative to P_c at $C_a = 40$ Pa for different soil water potentials (P_s).

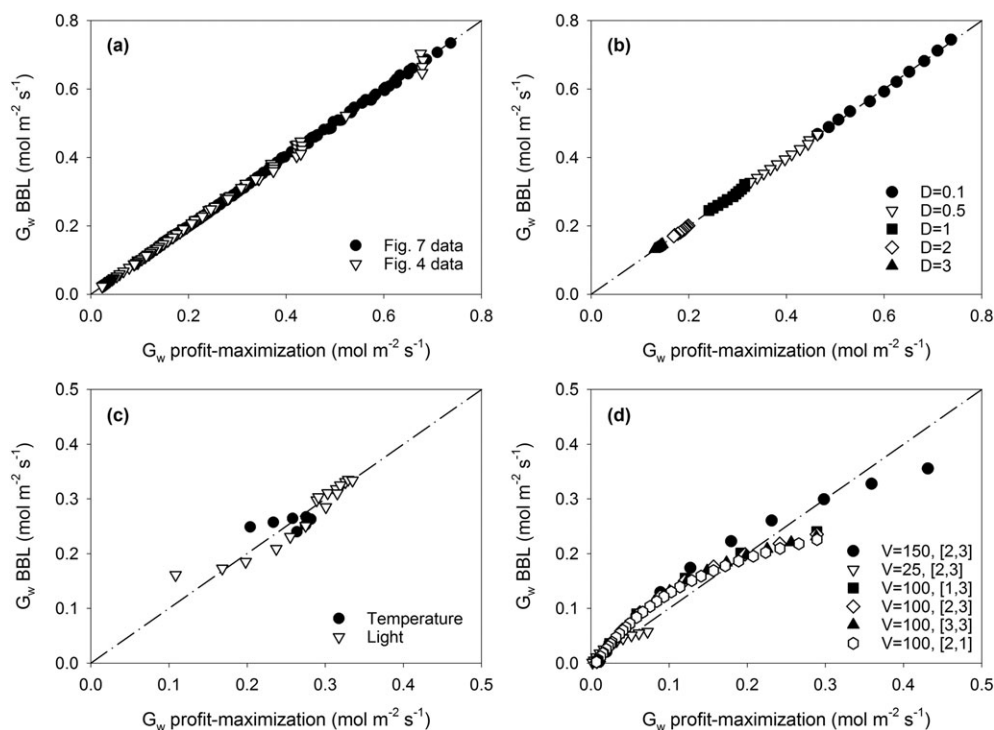


Figure 8. Best-fit between the leaf diffusive stomatal conductance (G_w) for profit-maximization and the Ball–Berry–Leuning equation (BBL, Eqn 12); r^2 values and BBL coefficients shown in Table 2. (a) Response to increasing leaf-air vapour pressure deficit (D_L). Open triangles are the six simulations from Fig. 4; solid symbols are the simulations from Fig. 7a (D_L responses at 11 ambient CO₂ (C_a) settings). (b) Response to C_a (at five different D_L settings in Fig. 7a). (c) Response to light and leaf temperature responses from Fig. 5. (d) Response to soil water potential (P_s) from six simulations in Fig. 6, where V is maximum carboxylation rate, $V_{\max25}$ ($\mu\text{mol s}^{-1}\text{m}^{-2}$) and bracketed numbers are [b,c] settings for the Weibull vulnerability curve (Eqn 1b).

(Fig. 8c; Table 2; r^2 0.91), with BBL predicting more gradual closure in low light. The temperature response was poorly fit (Fig. 8c; Table 2; r^2 0.12) with BBL over-predicting G_w at low temps and under-predicting at high. However, this simulation represents an unusual challenge to BBL in that it is unlikely in nature to have leaf temperature varying independently of D_L . The BBL was not intended to capture the P_s response, which is reflected in its poor fit to the Fig. 6 simulations (Fig. 8d, Table 2). Although the r^2 averaged 0.94, there was consistent non-linearity because BBL under-predicted the rate of stomatal closure with P_s . The a' coefficient was quite variable across the P_s simulations, and G_o was consistently negative (Table 2).

DISCUSSION

Our purpose was to present the rationale and quantitative proof of concept for a novel and synthetic model for stomatal responses at the leaf scale. The profit-maximizing scheme efficiently predicted a wide range of stomatal (G_w) and xylem pressure (P_c) responses to environmental factors (Figs 3–7) without recourse to *ad hoc* empirical coefficients. The instantaneous $E(P_c)$ and $A(P_c)$ functions (Fig. 1a,c, blue E and green A curves) are calculated from established hydraulic and biochemical processes initialized by measurable traits (Table 1). They represent the full spectrum of steady-state water-for-carbon exchange options available at a given instant. The supply $E(P_c)$ function is a defensible proxy for the increasing cost of losing

more water: every additional increment in stomatal conductance sooner or later requires an ever-increasing drop in P_c , owing to ever-declining canopy hydraulic conductance, which accelerates the approach to certain desiccation at E_{crit} . Clearly, either extreme of the $A(P_c)$ and $E(P_c)$ exchange spectrum is non-adaptive, and the plant should be somewhere in the middle. The optimization criterion is straightforward: at a given instant, stomata should maximize the difference between photosynthetic gain and hydraulic cost. Both gain and cost metrics are normalized to zero at stomatal closure and 1 at the maximum over the hydraulically permissible range of stomatal opening for that instant. This simple algorithm predicts a host of plant responses (e.g. E , A , G_w , G_c , P_c , T_L , C_i) to any combination of plant and environmental factors (e.g. k_{\max} , $V_{\max25}$, cavitation vulnerability, leaf size, P_s , D , T_A , C_a , u , Q).

The general congruence between the optimization scheme and the hydraulics-only approach (Eqn 3; Sperry & Love 2015; Sperry *et al.* 2016) results from the common use of the $E(P_c)$ derivative (k_c) as the key model factor that constrains stomatal opening. The largest qualitative difference is that optimization predicts non-isohydric P_c response to increasing D_L , which is arguably more realistic than the strict D_L isohydry predicted by the hydraulic model (Fig. 4b,c). Nevertheless, the hydraulic model appears to explain much of the variation in stomatal responses (G_w and P_c) to D and P_s (Sperry *et al.* 2016), and should be useful when the additional photosynthetic parameters required for the optimization scheme are

unavailable, and CO₂ and light do not vary substantially. All of its advantages in capturing the isohydric-to-anisohydric spectrum (e.g. Fig. 6d; and see Sperry *et al.* 2016), and the coupled responses to D_L and P_s (Figs 4 & 6), carry over in the optimization model. However, the optimization model captures the most complete suite of stomatal responses because G_w responds to A . This allows it to predict additional responses to T_A , Q and C_a (Figs 5 & 7).

The comparison to the Ball–Berry–Luening (Leuning 1995) model (BBL) represents a ‘zero-order’ test of the optimization model. The BBL fit was essentially perfect for the stomatal response to D_L and C_a (Figs 4 & 7). This result was anticipated by the BBL form of theoretical derivations for profit maximization (Wolf *et al.* 2016). The BBL congruency suggests that the trends in Figs 4 (closure at high D_L) and 7 (opening at low C_a , closure at high C_a) are quantitatively as well as qualitatively consistent with observations. The advantage of the optimization approach over BBL (or other empirical models) is the absence of *ad hoc* fitting parameters (e.g. Table 2) and its basis in trait and process. Even more importantly, the optimization model applies equally well to dry soil (e.g. Fig. 6a,c). The BBL model lacks any parameter for capturing the G_w response to drying soil (Eqn 12; Dammour *et al.* 2010), and under-predicts stomatal closure relative to the optimization model (Fig. 8d). This critical defect is often patched up in ecosystem models by the addition of more *ad hoc* functions and coefficients (Jarvis 1976; Powell *et al.* 2013). But the optimization model provides a simpler and more powerful alternative. Its integration of photosynthesis and hydraulics predicts not only gas exchange and energy balance, but the accompanying water relations and hydraulic status. As the rapidly growing literature on drought induced tree mortality suggests, metabolic, temperature and hydraulic stresses are inextricably intertwined during drought (McDowell *et al.* 2008; Rowland *et al.* 2015; Anderegg *et al.* 2016). Models need to represent their integration to best predict responses to environmental change (McDowell *et al.* 2013).

Additional evidence for the optimization model comes from its prediction of a tightly coupled coordination between k_{max} , G_{max} and V_{max25} (Fig. 3). This is consistent with an abundance of data showing a positive relationship between k_{leaf} and V_{max} (Clearwater & Meinzer 2001; Brodribb *et al.* 2002; Brodribb *et al.* 2005; Brodribb *et al.* 2007; Campanello *et al.* 2008; Brodribb 2009; Brodribb & Feild 2010; Limousin *et al.* 2013; Novick *et al.* 2016). The coordination between hydraulic and photosynthetic capacity emerges from the assumption that C_i/C_a is maintained at a set value under favourable conditions. A constant C_i/C_a target was also proposed as a carbon-for-water transport optimization criterion by Prentice *et al.* (2014), and previous modelling has demonstrated its theoretical link to plant hydraulic properties (Katul *et al.* 2003). The optimal k_{max} settings also correspond to leaf area-specific hydraulic conductances within the measured range (5–65 mmol s⁻¹ m⁻² MPa; assuming leaves are 25% of plant resistance at full hydration; Sack & Tyree 2005). The further prediction that k_{max} should increase with vulnerability to cavitation (Fig. 3b) is consistent with generally observed trends (Gleason *et al.* 2015). Interestingly, however, this trend is predicted independently of any safety versus efficiency trade-off at the xylem

level. Instead, it emerges from vulnerable xylem limiting the soil-canopy ΔP , thus requiring higher k_{max} to achieve the G_w required to keep A and C_i at optimal levels (Fig. 3a).

Our optimization criterion, that of instantaneously maximizing carbon gain (β) minus hydraulic cost (θ ; Eqn 11; Wolf *et al.* 2016), is importantly different from the Cowan–Farquhar maximization of carbon gain for a fixed amount of water loss. The $\partial E/\partial A = \lambda'$ target for stomatal regulation in the Cowan–Farquhar scheme is unspecified, which prevents direct comparison of G_w . But the response *shape* can be compared by setting $\lambda' = \partial E/\partial A$ at the initial G_w for profit maximization, and plotting the alternative G_w trajectory that maintains λ' instead of profit maximization. When soil is wet, the G_w response to D_L can be quite similar (Fig. 9a, $P_s = 0$ curves; $V_{max25} = 100 \mu\text{mol s}^{-1} \text{m}^{-2}$, $T_A = 30^\circ\text{C}$), which is consistent with support for a near-constant $\partial E/\partial A$ over diurnal time frames of favourable soil moisture (e.g. Farquhar *et al.* 1980). It is also consistent with relatively low hydraulic cost under these conditions. However, as soil dries, the new λ' setting (reduced to match the lower initial G_w) predicts more severe closure with D_L (even to $G_w \approx 0$) and more conservative water use versus profit maximization, which predicts $\partial E/\partial A$ should rise with D_L (rather than stay constant). Such a rise has been observed (Thomas *et al.* 1999; but see Buckley *et al.* 2016) and is also predicted if T_L increases with D_L beyond the photosynthetic optimum (simulations not shown). The response to P_s (constant D) is dramatically different in the two schemes: maintaining λ' results in no stomatal closure and premature hydraulic failure (Fig. 9b, desiccation at the asterisk). Profit maximization predicts a strong closure response (and declining $\partial E/\partial A$) because of the rising cost of extracting water from drying soil. The reduction in λ' with drier soil has been anticipated and observed, although its *a priori* specification remains very difficult (Cowan 1982; Makala *et al.* 1996; Thomas *et al.* 1999; Manzoni *et al.* 2011; Manzoni *et al.* 2013). The CO₂ response is also dramatically different: as C_a is increased from 15 Pa, maintaining λ' initially results in stomatal *opening*, versus the expected closure response as predicted by profit maximization (Fig. 9c). This wrong-way response is consistent with a further need to adjust λ' with C_a (Katul *et al.* 2010). Given their often divergent stomatal responses, it should be possible to deduce which optimization criterion is being followed (λ' versus profit maximization) by analysing data sets of gas exchange and xylem pressure with strong variation in D , P_s and C_a (Wolf *et al.* 2016; Anderegg, W.R.L. unpublished).

Our optimization model awaits validation against specific data sets. But its qualitative consistency with observation and quantitative agreement with BBL is promising. It has theoretical and practical advantages over the Cowan–Farquhar scheme: it poses an optimization criterion consistent with competition for water, it is readily calculated from measurable traits and it automatically responds in realistic ways to the gamut of environmental cues. The profit maximization scheme can be integrated into existing stand- and ecosystem models, including the hydraulically sophisticated TREES (Mackay *et al.* 2015). The hope is that these larger-scale models will be significantly improved by a stomatal control routine that is based on physiologically relevant traits and processes, yet computationally tractable and lean in parameters.

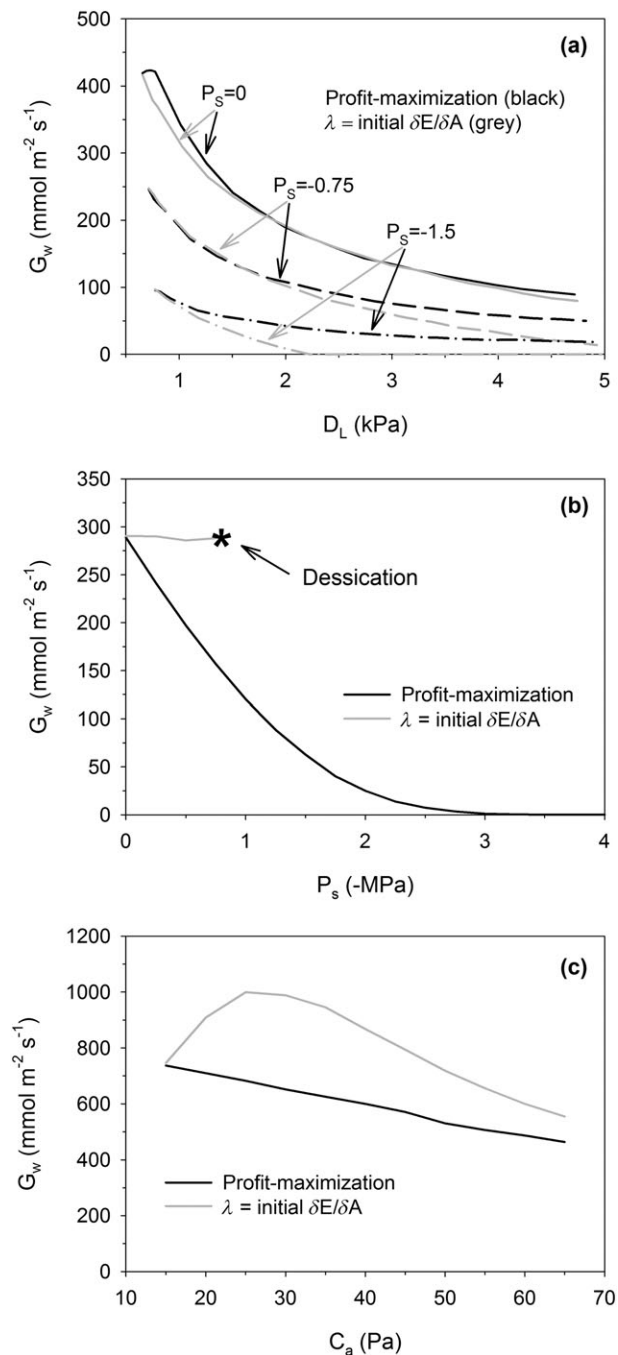


Figure 9. The response of leaf diffusive conductance (G_w) for profit maximization (black curves) versus the constrained optimization of Cowan & Farquhar (1977; grey curves) where marginal water use efficiency ($\lambda' = \delta E / \delta A$) is constant at the initial value for profit maximization. (a) The response to leaf-air vapour pressure deficit (D_L) at three soil water potentials ($P_s = 0, -0.75, -1.5$ MPa). (b) Response to P_s ; asterisk denotes point of hydraulic failure and canopy desiccation. (c) Response to ambient CO₂ concentration (C_a).

ACKNOWLEDGMENTS

We thank Plant Cell and Environment for this special issue invitation. Funding was from NSF-IOS-1450650 and NSF-IOS-1450679. Dr. Gabriel Katul (Duke University) generously

provided feedback on an early draft, and we benefitted from informative discussions with Fred Adler (University of Utah), Belinda Medlyn (Western Sydney University) and an anonymous referee provided excellent review feedback.

REFERENCES

- von Allmen A.I., Sperry J.S. & Bush S.E. (2015) Contrasting whole-tree water use, hydraulics, and growth in a co-dominant diffuse-porous vs. ring-porous species pair. *Trees Structure and Function* **29**, 717–728.
- Anderegg W.R.L., Flint A., Huang C., Flint L., Berry J.A., Davis F., Sperry J.S. & Field C.B. (2015) Tree mortality predicted from drought-induced vascular damage. *Nature Geoscience* **8**, 367–371.
- Anderegg W.R.L., Klein T., Bartlett M., Sack L., Pellegrini B., Choat B. & Jansen S. (2016) Meta-analysis reveals that hydraulic traits explain cross-species patterns of drought-induced tree mortality across the globe. *Proceedings of the National Academy of Sciences of the United States of America* **113**, 5024–5029.
- Bernacchi C.J., Singsaas E.L., Pinetel C., Portis A.R. & Long S.P. (2001) Improved temperature response functions for models of Rubisco-limited photosynthesis. *Plant, Cell & Environment* **24**, 253–259.
- Bonan G.B., Williams M., Fisher R.A. & Oleson K.W. (2014) Modeling stomatal conductance in the earth system: linking leaf water-use efficiency and water transport along the soil-plant-atmosphere continuum. *Geosciences Model Development* **7**, 2193–2222.
- Brodribb T.J. (2009) Xylem hydraulic physiology: the functional backbone of terrestrial plant productivity. *Plant Science* **177**, 245–251.
- Brodribb T.J. & Feild T.S. (2010) A surge in leaf photosynthetic capacity during early angiosperm diversification. *Ecology Letters* **13**, 175–183.
- Brodribb T.J., Feild T.S. & Jordan G.J. (2007) Leaf maximum photosynthetic rate and venation are linked by hydraulics. *Plant Physiology* **144**, 1890–1898.
- Brodribb T.J., Holbrook N.M. & Gutierrez M.V. (2002) Hydraulic and photosynthetic co-ordination in seasonally dry tropical forest trees. *Plant, Cell & Environment* **25**, 1435–1444.
- Brodribb T.J., Holbrook N.M., Zwieniecki M.A. & Palma B. (2005) Leaf hydraulic capacity in ferns, conifers, and angiosperms: impacts on photosynthetic maxima. *New Phytologist* **165**, 839–846.
- Buckley T.N., Sack L. & Farquhar G.D. (2016) Optimal plant water economy. *Plant, Cell & Environment*. DOI:10.1111/pce.12823.
- Campanello P.L., Gatti M.G. & Goldstein G. (2008) Coordination between water-transport efficiency and photosynthetic capacity in canopy tree species at different growth irradiances. *Tree Physiology* **28**, 85–94.
- Campbell G.S. & Norman J.N. (1998) *An Introduction to Environmental Biophysics* 2nd edn. Springer, New York.
- Clearwater M.J. & Meinzer F.C. (2001) Relationship between hydraulic architecture and leaf photosynthetic capacity in nitrogen-fertilized *Eucalyptus grandis* trees. *Tree Physiology* **21**, 683–690.
- Collatz G.J., Ball J.T., Griwet C. & Berry J.A. (1991) Physiological and environmental regulation of stomatal conductance, photosynthesis and transpiration: a model that includes a laminar boundary layer. *Agricultural and Forest Meteorology* **54**, 107–136.
- Collatz G.J., Ribas-Carbo M. & Berry J.A. (1992) Coupled photosynthesis-stomatal conductance model for leaves of C4 plants. *Australian Journal of Plant Physiology* **19**, 519–538.
- Cowan I.R. (1982) Regulation of water use in relation to carbon gain in higher plants. In *Physiological Plant Ecology II. Encyclopedia of Plant Physiology* (eds Lange O.L., Nobel P.S., Osmond C.B. & Ziegler H.), Vol. **12B**, pp. 589–613. Springer-Verlag, Berlin.
- Cowan I.R. & Farquhar G.D. (1977) Stomatal function in relation to leaf metabolism and environment. In *Integration of Activity in the Higher Plant* (ed Jennings D.H.), pp. 471–505. Cambridge University Press, Cambridge.
- Darmour G., Simonneau T., Cochard H. & Urban L. (2010) An overview of models of stomatal conductance at the leaf level. *Plant, Cell & Environment* **33**, 1419–1438.
- Farquhar G.D., Schulze E.D. & Kupperts M. (1980) Responses to humidity by stomata of *Nicotiana glauca* L. and *Corylus avellana* L. are consistent with the optimization of carbon dioxide uptake with respect to water loss. *Australian Journal of Plant Physiology* **7**, 315–327.
- Feild C.B. & Holbrook N.M. (1989) Catastrophic xylem failure: life at the brink. *Trends in Ecology and Evolution* **4**, 124–126.

- van Genuchten M.T. (1980) A closed form equation for predicting the hydraulic conductivity of unsaturated soils. *Soil Science Society of America Journal* **44**, 892–898.
- Givnish T.J. (1986) Optimal stomatal conductance, allocation of energy between leaves and roots, and the marginal cost of transpiration. In *On the Economy of Plant Form and Function* (ed Givnish T.J.), pp. 171–213. Cambridge University Press, Cambridge.
- Gleason S.M., Westoby M., Jansen S., Choat B., Hacke U.G., Pratt R.B., ... Zanne A.E. (2015) Weak tradeoff between xylem safety and xylem-specific hydraulic efficiency across the world's woody plant species. *New Phytologist* **209**, 123–136.
- Hetherington A.M. & Woodward F.I. (2003) The role of stomata in sensing and driving environmental change. *Nature* **424**, 901–908.
- Jarvis P.G. (1976) The interpretation of the variations in leaf water potential and stomatal conductance found in canopies in the field. *Philosophical Transactions of the Royal Society London, Series B* **273**, 593–610.
- Katul G.G., Leuning R. & Oren R. (2003) Relationship between plant hydraulic and biochemical properties derived from a steady-state coupled water and carbon transport model. *Plant, Cell & Environment* **26**, 339–350.
- Katul G.G., Manzoni S., Palmroth S. & Oren R. (2010) A stomatal optimization theory to describe the effects of atmospheric CO₂ on leaf photosynthesis and transpiration. *Annals of Botany* **105**, 431–442.
- Kukowski K., Schwinnig S. & Schwartz B. (2013) Hydraulic responses to extreme drought conditions in three co-dominant tree species in shallow soil over bedrock. *Oecologia* **171**, 819–830.
- Leuning R. (1995) A critical appraisal of a coupled stomatal-photosynthesis model for C3 plants. *Plant, Cell & Environment* **18**, 339–357.
- Leuning R. (2002) Temperature dependence of two parameters in a photosynthesis model. *Plant, Cell & Environment* **25**, 1205–1210.
- Limousin J., Bickford C., Dickman L., Pangle R., Hudson P., Boutz A., ... McDowell N. (2013) Regulation and acclimation of leaf gas exchange in a piñon-juniper woodland exposed to three different precipitation regimes. *Plant, Cell & Environment* **36**, 1812–1825.
- Mackay D.S., Roberts D.E., Ewers B.E., Sperry J.S., McDowell N. & Pockman W. (2015) Interdependence of chronic hydraulic dysfunction and canopy processes can improve integrated models of tree response to drought. *Water Resources Research* **51**. DOI:10.1002/2015WR017244.
- Makala A., Berninger F. & Hari P. (1996) Optimal control of gas exchange during drought: theoretical analysis. *Annals of Botany* **77**, 461–468.
- Manzoni S., Vico G., Katul G., Fay P.A., Polley W., Palmroth S. & Porporato A. (2011) Optimizing stomatal conductance for maximum carbon gain under water stress: a meta-analysis across plant functional types and climates. *Functional Ecology* **25**, 456–467.
- Manzoni S., Vico G., Porporato A., Palmroth S. & Katul G. (2013) Optimization of stomatal conductance for maximum carbon gain under dynamic soil moisture. *Advances in Water Resources* **62**, 90–105.
- McDowell N., Fisher R.A., Xu C., Domec J.C., Holttla T., Mackay D.S., ... Pockman W.T. (2013) Evaluating theories of drought-induced vegetation mortality using a multimodel-experimental framework. *New Phytologist* **200**, 304–321.
- McDowell N., Pockman W.T., Allen C.D., Breshears D.D., Cobb N., Kolb T., ... Yezpe E.A. (2008) Mechanisms of plant survival and mortality during drought. Why do some plants survive while others succumb to drought? *New Phytologist* **178**, 719–739.
- Medlyn B.E., Dreyer E., Ellsworth D.S., Forstreuter M., Harley P.C., Kirschbaum M.U.F., ... Loustau D. (2002) Temperature response of parameters of a biochemically based model on photosynthesis. II. A review of experimental data. *Plant, Cell & Environment* **25**, 1167–1179.
- Medlyn B.E., Duursma R.A., Eamus D., Ellsworth D.S., Prentice I.C., Barton C.V.M., ... Wingate L. (2011) Reconciling the optimal and empirical approaches to modelling stomatal conductance. *Global Change Biology* **17**, 2134–2144.
- Morison J.I.L. (1987) Intercellular CO₂ concentration and stomatal response to CO₂. In *Stomatal Function* (eds Zeiger E., Cowan I.R. & Farquhar G.D.), pp. 229–251. Stanford University Press, Stanford.
- Novick K.R., Miniat C.F. & Vose J.M. (2016) Drought limitations to leaf-level gas exchange: results from a model linking stomatal optimization and cohesion-tension theory. *Plant, Cell & Environment* **39**, 583–596.
- Neufeld H.S., Grantz D.A., Meinzer F.C., Goldstein G., Crisosto G.M. & Crisosto C. (1992) Genotypic variability in vulnerability of leaf xylem to cavitation in water-stressed and well-irrigated sugarcane. *Plant Physiology* **100**, 1020–1028.
- Paul M.J. & Foyer C.H. (2001) Sink regulation of photosynthesis. *Journal of Experimental Botany* **52**, 1383–1400.
- Powell T., Galbraith D., Christoffersen B., Harper A., Imbuzeiro H., Rowland L., ... Moorcroft P. (2013) Confronting model predictions of carbon fluxes with measurements of Amazon forests subjected to experimental drought. *New Phytologist* **200**, 350–365.
- Prentice I.C., Dong N., Gleason S.M., Maire V. & Wright I.J. (2014) Balancing the costs of carbon gain and water transport: testing a new theoretical framework for plant functional ecology. *Ecology Letters* **17**, 82–91.
- Rowland L., da Costa A.C.L., Galbraith D.R., Oliveira R.S., Binks O.J., Oliveira A.A., ... Meir P. (2015) Death from drought in tropical forests is triggered by hydraulics not carbon starvation. *Nature* **528**, 119–122.
- Sack L. & Tyree M.T. (2005) Leaf hydraulics and its implications in plant structure and function. In *Vascular Transport in Plants* (eds Holbrook N.M. & Zwieniecki M.A.), pp. 93–114. Elsevier/Academic Press, Oxford.
- Schulze E.D. & Hall A.E. (1982) Stomatal responses water loss and CO₂-assimilation rates of plant in contrasting environments. In *Physiological Plant Ecology II. Water Relations and Carbon Assimilation* (eds Lange O.L., Nobel P.S., Osmond C.B. & Ziegler H.), pp. 181–230. Springer Verlag, Berlin.
- Sparks J.P. & Black R.A. (1999) Regulation of water loss in populations of *Populus trichocarpa*: the role of stomatal control in preventing xylem cavitation. *Tree Physiology* **19**, 453–459.
- Sperry J.S., Adler F.R., Campbell G.S. & Comstock J.P. (1998) Limitation of plant water use by rhizosphere and xylem conductance: results from a model. *Plant, Cell & Environment* **21**, 347–359.
- Sperry J.S. & Love D.M. (2015) Tansley review: What plant hydraulics can tell us about plant responses to climate-change droughts. *New Phytologist* **207**, 14–27.
- Sperry J.S., Wang Y., Wolfe B., Mackay D.S., Anderegg W.R.L., McDowell N.G. & Pockman W.T. (2016) Pragmatic hydraulic theory predicts stomatal responses to climatic water deficits. *New Phytologist* **212**, 577–589.
- Thomas D.S., Eamus D. & Bell D. (1999) Optimization theory of stomatal behaviour II. Stomatal responses of several tree species of north Australia to changes in light, soil and atmospheric water content and temperature. *Journal of Experimental Botany* **50**, 393–400.
- Tombesi S., Nardini A., Frioni T., Socolini M., Zadra C., Farinelli D., ... Palliotti A. (2015) Stomatal closure is induced by hydraulic signals and maintained by ABA in drought-stressed grapevine. *Scientific Reports* **5**, 12449.
- Tyree M.T. & Sperry J.S. (1988) Do woody plants operate near the point of catastrophic xylem dysfunction caused by dynamic water stress? Answers from a model. *Plant Physiology* **88**, 574–580.
- Williams M., Rastetter E.B., Fernandes D.N., Goulet M.L., Wofsy S.C., Shaver G.R., ... Nadelhoffer K.J. (1996) Modelling the soil-atmosphere continuum in a *Quercus-Acer* stand at Harvard Forest: the regulation of stomatal conductance by light, nitrogen and soil/plant hydraulic properties. *Plant, Cell & Environment* **19**, 911–927.
- Wolf A., Anderegg W.R.L. & Pacala S. (2016) Optimal stomatal behavior with competition for water and risk of hydraulic impairment. *Proceedings of the National Academy of Sciences of the United States of America*. In Press.
- Wong S.C., Cowan I.R. & Farquhar G.D. (1979) Stomatal conductance correlates with photosynthetic capacity. *Nature* **282**, 424–426.

Received 11 July 2016; received in revised form 28 September 2016; accepted for publication 6 October 2016

SUPPORTING INFORMATION

Additional Supporting Information may be found in the online version of this article at the publisher's web-site:

Figure S1. Examples of how specific plant- and environmental parameters shifts the gain-cost ($\beta-\theta$) optimization.

Figure S2. Example of how an exponential vulnerability curve shifts the gain-cost ($\beta-\theta$) optimization in wet versus dry soil.